Supplementary Information

Surface Fully Functionalized Metal Chalcogenides Nanowire for Highly Sensitive H_2S Sensing

Ying-Xue Jin[a,d], Jie Chen[a,c], Yong-Jun Chen[a], Wei-Hua Deng[a], Xiao-Liang Ye[a], Guan-E Wang[a,d*], Gang Xu[a,b,d*]

[a] State Key Laboratory of Structural Chemistry, Fujian Institute of Research on the Structure of Matter, Chinese Academy of Sciences, Fuzhou, Fujian 350002, China.

[b] Science & Technology Innovation Laboratory for Optoelectronic Information of China Fuzhou, Fujian 350108, China.

[c] College of Chemistry, Fuzhou University, Fuzhou, Fujian 350116, China.

[d] University of Chinese Academy of Sciences (UCAS), Beijing 100049, China.

1. Experimental Section

Materials: Cadmium acetate dihydrate was purchased from adamas-beta, 4-aminothiophenol was purchased from Aladdin, Potassium bromide was purchased from Macklin, ethanol (EtOH) was all derived from chemical reagents Chinese medicine Holdings Limited, China. All solvents and reagents were purchased without further purification. Ag-Pd interdigitated electrodes (the effective width: 7 mm, length: 4 mm, channel length: 200 μm) were purchased from Beijing Elite Tech, Co. (China). Water was purified by mil-q purification system.

Characterization: Powder X-ray diffraction (PXRD) of the Cd-ATP sample was recorded on a Rigaku SmartLab (Japan) equipped with Cu Kα radiation (λ = 1.54060 Å). Scanning electron microscopy (SEM, ZEISS Sigma 500) and transmission electron microscope (TEM, FEI TALOS F200X G2) were applied to investigate the morphology of the samples. Atomic force microscope (AFM) images were collected on a Bruker Dimension ICON atomic force microscope. Cd-ATP films were used for UV-vis diffuse reflectance spectra measurement operated on a Lambda 900 (PerkinElmer, USA). FT-IR spectra were recorded from KBr pellets in the range 4000 - 400 cm^{-1} on Nicolet 170 SXFT-IR spectrometer. A Nicolet 6700 infrared spectrometer equipped with an MCT-A detector was used to study the mechanism of the gas-sensitive reaction. The electrical performance of the device was measured using a Keithley 4200 (USA) semiconductor characterization system. X-ray photoelectron spectroscopy (XPS) measurements were performed on an American Thermo-VG Scientific ESCALAB 250 Xi XPS system with Al Kα radiation as the exciting source. Electron paramagnetic resonance (EPR) measurements were conducted on a Bruker A300 spectrometer in the visible-light mode, DMPO was used as a radical trapper.

Synthesis of Cd-ATP single crystal: A mixture of Cadmium acetate dihydrate (0.0530 g, 0.2 mmol), 4-aminothiophenol (160 μL, 0.8 mmol), Potassium bromide (0.0119 g, 0.1 mmol), ethanol (3 mL) and DI water (5 mL) was heated at 358 K for 48 hours in oven. After filtering, washing, and air drying, PXRD analysis confirmed that the white sample was crystalline.

Preparation of Cd-ATP nanowire mesh films: A mixture of Cadmium acetate dihydrate (0.0530 g, 0.2 mmol), 4-aminothiophenol (160 μL, 0.8 mmol), Potassium bromide (0.0119 g, 0.1 mmol), ethanol (15 mL) and DI water (25 mL) put into a 50 mL glass bottle, sonicated for 30 min in a 100 W ultrasonic machine, and then placed in a stirrer at 293 K. After stirring for

24 hours, a mercerizing phenomenon appeared, and a dense film was obtained by vacuum filtration. The cleaned mesh film was shaken slightly in the filter paper. The purchased Ag-Pd interdigital electrode was used to lift the film and air dried.

Measurement of gas sensor: Sensing performances of Cd-ATP toward all gases were evaluated in a homemade instrument system developed in our early work. [1] As shown in Figure S1, at room temperature, the system consists of piping, a gas mixing device, a test chamber and a digital source meter. The gas flow of air and analytes was controlled at 600 sccm by mass flow controllers (MFC). The electrical signal was recorded by using Keithley 2602B Sourcemeter in real-time. To simulate the actual operating conditions of the device, synthetic air (79% nitrogen + 21% oxygen) was used as the purge and standard carrier gas. The purge gas was introduced for 1 h prior to the test to remove any other gas molecules that might be adsorbed on the material surface and to stabilize the baseline. In addition, a xenon arc lamp (PLS-SXE300D) with a light intensity of 360 K lx and a filter (420 - 760 nm) was utilized as an irradiation source above the test chamber.

Calculations of response, response/recovery time and coefficient of variation: The response (R) of Cd-ATP to the gases was determined by detecting the changes in resistance and defined as $R\ (\%) = (r_{gas}/r_{air} - 1) \times 100$ for reducing gases (where r_{air} and r_{gas} are the resistance of Cd-ATP in air and target gas, respectively). The response and recovery times for Cd-ATP were acquired as the times taken to achieve 90% of the total resistance change. The coefficient of variation (CV) was defined as: $CV = R_{SD}/R_{average} \times 100\%$, where R_{SD} and $R_{average}$ are the standard deviation (SD) and the average value of responses with five successive cycles.

H_2S in situ FT-IR spectra: In order to investigate the mechanism of the gas-sensitive response, the interaction of gas molecules with the material surface was investigated by a diffuse reflectance infrared Fourier transform spectroscopy (DRIFTS) test. Before testing, a raw diffuse reflectance infrared absorption spectrum of KBr was acquired as a background for sample testing. The raw spectra of KBr were collected by passing high purity argon gas at 80 °C for 1 h to remove adsorbed moisture and other gas molecules, and then passing purge synthetic air after the sample and sample chamber had cooled to room temperature for 30 min. Cd-ATP nanowire samples (60 mg) were then loaded into the sample compartment and the synthetic air purging operations were repeated. Then, the sample was treated with a filter

(420 - 760 nm) at a xenon arc lamp light intensity of 360 K lx (PLS-SXE300D) and the original spectrum of the sample was first collected as a background. Next, 100 ppm of H_2S was injected and collected its spectrum. Spectra were collected at a resolution of 4.0 cm^{-1} with 128 scans.

Adsorption isotherm of Cd-ATP for hydrogen sulfide: The sample was dispersed by ethanol and then loaded onto the front of the micro-cantilever of the chip through a micro-cantilever microscope and tested by Chip-based resonant micro-cantilever molecular adsorption analyzer. After sufficient drying, the amount of hydrogen sulfide adsorbed by the sample was measured by detecting the vibration frequency of the cantilever beam at different concentrations of hydrogen sulfide from 10 ppm to 250 ppm. The adsorption of hydrogen sulfide by Cd-ATP at 25°C and 35°C were collected and plotted in Figure S9 and fitted by Langmiur adsorption. Then, by reading the partial pressure (p_1 and p_2) of hydrogen sulfide required for different temperatures at the same adsorption volume, we calculated the heat of adsorption (ΔH: under isothermal and isobaric conditions) of the sample on hydrogen sulfide through the Arrhenius equation:

$$\Delta H = \frac{RT_1T_2}{T_2 - T_1} ln\frac{p_1}{p_2}$$

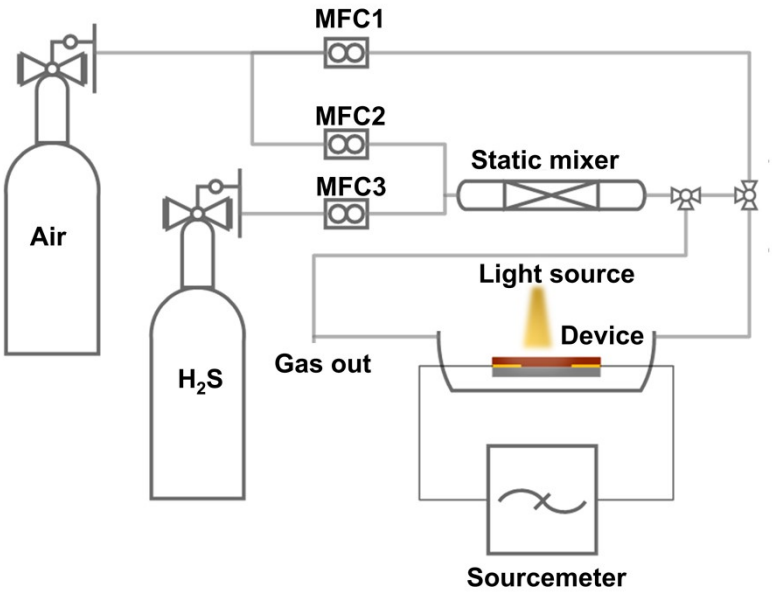

Figure S1. Homemade gas sensing test system.

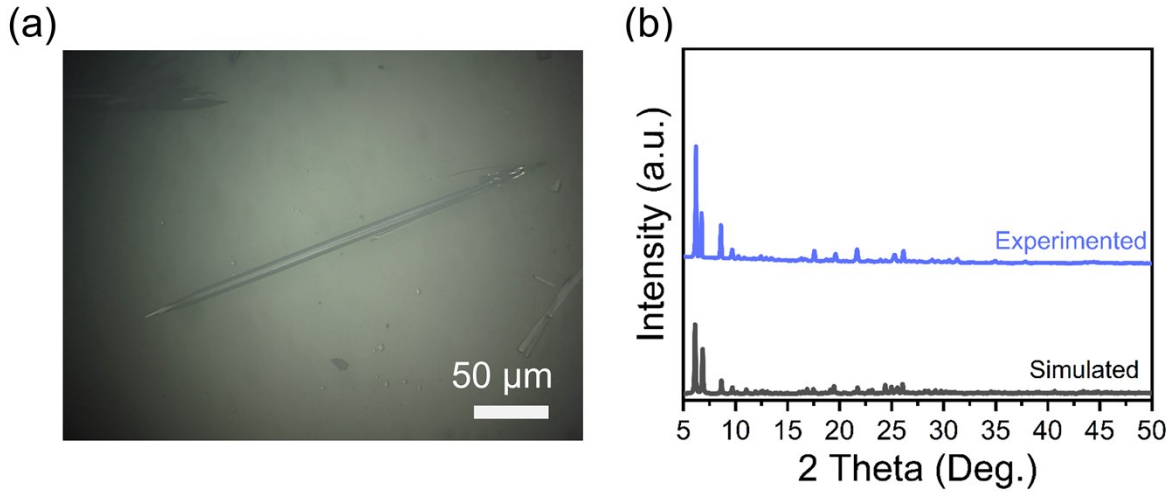

Figure S2. (a) Photograph of Cd-ATP single crystal. (b) PXRD of Cd-ATP powder.

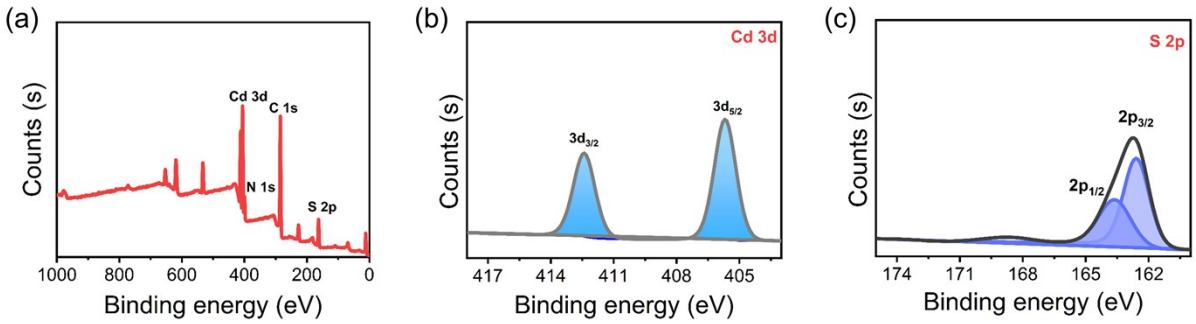

Figure S3. XPS spectra of Cd-ATP nanowires.

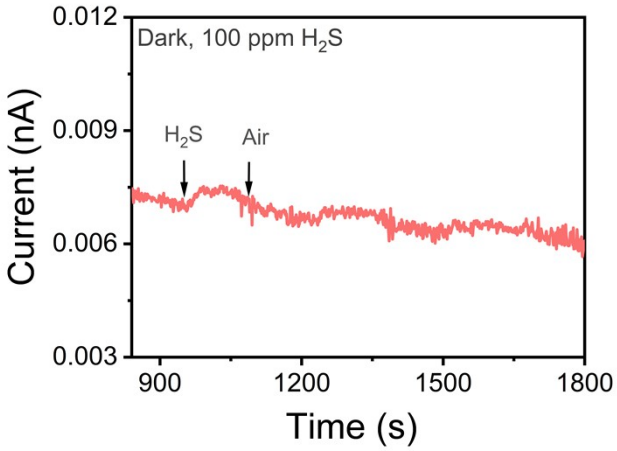

Figure S4. Gas sensing of Cd-ATP nanowire mesh film under dark condition.

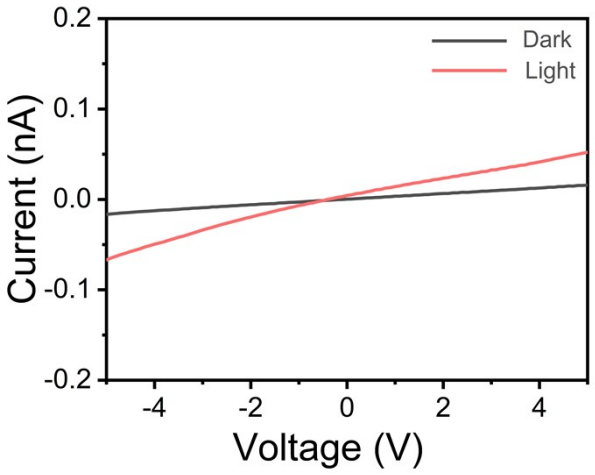

Figure S5. *I–V* characteristics of Cd-ATP nanowire mesh film under dark and light condition.

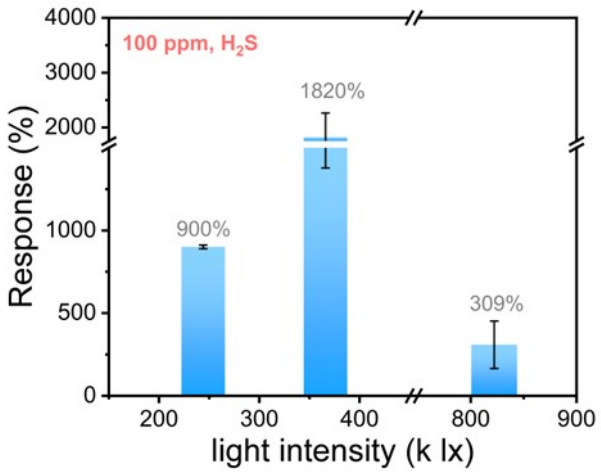

Figure S6. Influence of Xenon light intensity to response of 10 ppm H_2S.

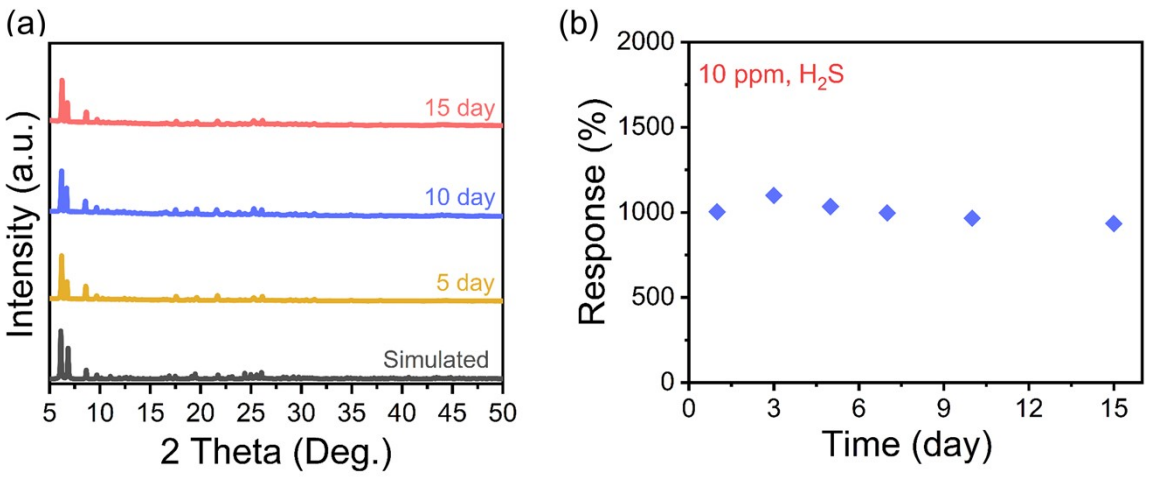

Figure S7. (a) PXRD of Cd-ATP nanowire film devices. (b) Long-term stability of Cd-ATP nanowire film devices to 10 ppm H_2S.

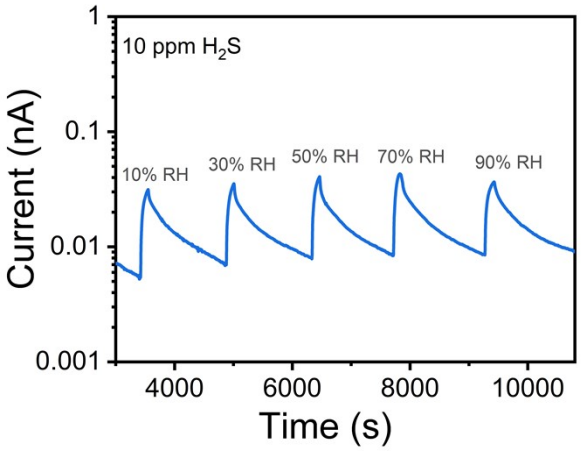

Figure S8. Response-recovery curve of Cd-ATP nanowire mesh films to 10 ppm H_2S under different humidity levels.

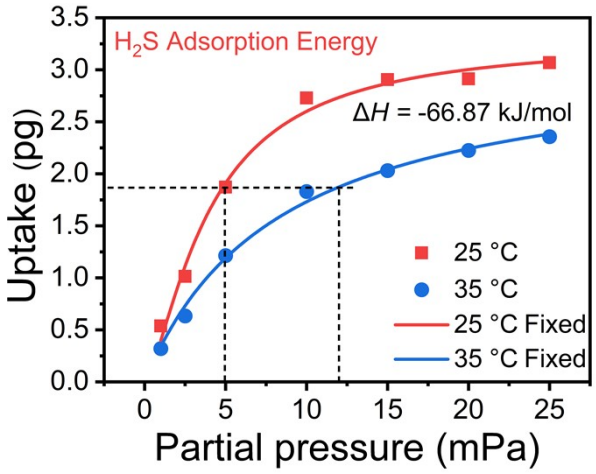

Figure S9. Adsorption isotherms of Cd-ATP nanowires for H_2S.

Table S1. Crystallographic data for Cd-ATP.

Crystal data	Cd-ATP
Empirical formula	$C_{54}H_{62}Cd_4KN_9O_3S_9$
Formula weight	1662.33
Temperature/K	99.99(10)
Crystal system	triclinic
Space group	*P*-1
a/Å	8.1350(10)
b/Å	18.4440(3)
c/Å	20.7198(3)
α/°	95.3890(10)
β/°	97.3830(10)
γ/°	96.4610(10)
V/Å^3	3044.90(8)
Z	2
ρ_{calc}/gcm^{-3}	1.803
μ/mm^{-1}	14.942
F(000)	1638.0
Radiation	Cu-K*α* (*λ* = 1.5418)
Reflections collected	34419
Independent reflections	10751 [R_{int} = 0.0516]
Data/restraints/parameters	10751/53/831
2theta range for data collection/°	4.326 to 133.196
Index ranges	-9 ≤ *h* ≤ 9, -20 ≤ *k* ≤ 21, -24 ≤ *l* ≤ 24
GOF on F^2	1.031
Final R indexes [I>=2σ (I)]	R_1 = 0.0693, wR_2 = 0.1904
Final R indexes [all data]	R_1 = 0.0787, wR_2 = 0.1967

[a]$R_1 = \Sigma||F_0|-|F_c||/\Sigma|F_0|$; [b]$wR_2 = [\Sigma w(F_0^2-F_c^2)^2/\Sigma w(F^2)^2]^{1/2}$

Table S2. Calculated and measured (with EA and ICP-AES) elemental mass percentage of Cd-ATP.

Element	Calculated weight percentage %	Measured weight percentage %
K	2.35%	2.47%
C	38.98%	39.98%
N	7.58%	7.69%
S	17.36%	18.23%
H	3.73%	3.38%

Table S3. Reported pure H_2S gas–sensing materials working at room temperature.

Material	LOD	Response	$t_{res.}$	*Ref.*
Cd-ATP	116.49 ppt	10 ppm / 965.68%	37.8 s	This work
Cu-MOF	1 ppm	100 ppm / 99%	8 s	2
$Ni_3(HITP)_2$ thin film	3 ppb	5 ppm / 2085%	12 min	3
TOM-$Cu_3(HITP)_2$ film	50 ppb	80 ppm / 7850%	3.5min	4
COF-DC-8	204 ppb	80 ppm / 80%	30 min	5
$Ni_3(HiTP)_2$	520 ppb	10 ppm / 65%	10 min	6
$Ni_3(HHTP)_2$	230 ppb	20 ppm / 20%	10 min	6
PNPA	100 ppb	10 ppm / 200%	1-10 min	7
NiPc-Cu	0.2 ppm	80 ppm / 98%	30 min	8
NiPc-Ni	0.5 ppm	80 ppm / 70%	30 min	8
CuO	100 ppb	5 ppm / 250%	60 s	9
In_2O_3	1 ppm	50 ppm / 24000%	140 s	10
CeO_2	50 ppb	100 ppm / 98%	100 s	11
Fe_2O_3	50 ppb	100 ppm / 3700%	250 s	12
CuO	1.52 ppb	5 ppb / 76.50%	102 s	13
ZnO	0.5 ppm	1 ppm / 29600%	246 s	14

References

1. M. S. Yao, W. X. Tang, G. E. Wang, B. Nath, G. Xu, *Adv. Mater.,* 2016, **28**, 5229-5234.

2. A. Ali, H. H. D. AlTakroori, Y. E. Greish, A. Alzamly, L. A. Siddig, N. Qamhieh, S. T. Mahmoud, *Nanomaterials.,* 2022, **12(6)**, 913.

3. T. Lee, J. O. Kim, C. Park, H. Kim, M. Kim, H. Park, I. Kim, J. Ko, K. Pak, S. Q. Choi, I. D. Kim, S. Park, *Adv. Mater.*, 2022, **34**, 2107696.

4. M. Miao, Z. Wang, Z. Guo, J. Xing, *Adv. Mater. Interfaces.*, 2022, **9**, 2101908.

5. Z. Meng, R. M. Stolz, K. A. Mirica, *J. Am. Chem. Soc.*, 2019, **141**, 11929-11937.

6. M. K. Smith, K. A. Mirica, *J. Am. Chem. Soc.*, 2017, **139**, 16759-16767.

7. V. V. Chabukswar, S. V. Bhavsar, A. S. Horne, K. Handore, V. B. Gaikwad, K. C. Mohite, *Macromol. Symp.*, 2013, **327**, 39-44.

8. Z. Meng, A. Aykanat, K. A. Mirica, *J. Am. Chem. Soc.*, 2018, **141**, 2046-2053.

9. N. S. Ramgir, S. K. Ganapathi, M. Kaur, N. Datta, K. P. Muthe, D. K. Aswal, S. K. Gupta, J. V. Yakhmi, *Sens. Actuators B Chem.*, 2010, **151**, 90-96.

10. Y. Wang, G. Duan, Y. Zhu, H. Zhang, Z. Xu, Z. Dai, W. Cai, *Sens. Actuators B Chem.*, 2016, **228**, 74-84.

11. Z. Li, X. Niu, Z. Lin, N. Wang, H. Shen, W. Liu, K. Sun, Y. Q. Fu, Z. Wang, *J. Alloys Compd.*, 2016, **682**, 647-653.

12. Huang, W. Chen, S. Zhang, Z. Kuang, D. Ao, N. R. Alkurd, W. Zhou, W. Liu, W. Shen, Z. Li, *Appl. Surf. Sci.*, 2015, **351**, 1025-1033.

13. Z. Huang, X. Wang, F. Sun, C. Fan, Y. Sun, F. Jia, G. Yin, T. Zhou, B. Liu, *Mater. Des.*, 2021, **201**, 109507.

14. Z. S. Hosseini, A. I. zad, A. Mortezaali, *Sens. Actuators B Chem.*, 2015, **207**, 865-871.